The Role of Applied Mathematics in Hydrodynamics for Ships and Floating Offshore Structures

Aad J. Hermans *

Abstract

The development of mathematical modelling to describe free-surface potential flow around ships and floating offshore structures is discussed giving an overview of recent developments and results, such as wave resistance, first and second order wave forces in seakeeping and offshore problems. It is shown that analytic methods are still useful or even necessary to analyse the properties of the numerical schemes, e.g. to evaluate numerical stability and numerical dispersion.

Keywords: free surface, wave resistance, seakeeping, panel method, dispersion

1 Introduction

At the end of the nineteenth century the first useful theoretical results in the field of ship motions and wave resistance are obtained. In 1861 William Froude studied the roll motions of ships in beam seas and Kriloff, in 1898, presented a general theory to describe the six degrees of motion. Their theory is based on severe physical simplifications, they considered the forces due to the pressure distribution of the undisturbed wave. With this so called Froude-Kriloff hypothesis the first comparisons of computed and measured ship motions are carried out. Michell succeeded in 1898 to incorporate the body disturbance to determine the wave resistance for a ship in a calm sea. His integral representation gives reasonable accurate results for the wave resistance of thin ships at higher Froude numbers, where the Froude number is defined as $F_n = U/\sqrt{gL}$, where U is the ship speed and L its length. For a long time the prediction of the wave resistance has been carried out by variants of Michell's integral. The results became unsatisfactory in the time one became interested in building large blunt vessels such as VLCC's. Their Froude number is low and especially near the bow the assumptions on which thin ship theory is based are violated. It turned out that the wave resistance is overestimated severely in this case. In the field of sea keeping the need for hydrodynamic coefficients and wave diffraction effects became apparent earlier and it was in 1929 that Lewis presented his two dimensional analytic theory to estimate the hydrodynamic coefficients for ship-like sections in short waves. Since then many extensions

*Faculty of Information Technology and Systems, Department of Applied Mathematics, TU Delft, Mekelweg 4, 2628 CD Delft, The Netherlands

and improvements are obtained by analytic methods.

Based on two-dimensional results *Korvin-Kroukovsky and Jacobs* (1957) developed a quasi three-dimensional so called strip theory to compute three dimensional ship motions, it takes care of forward speed effects in an aproximate way. This method is extended by several authors and leads to acceptable results for many applications. At this moment it is still in use and sometimes the results are superior to computations by fully three-dimensional codes.

In the field of aerodynamics *Hess and Smith* (1962) demonstrated successfully the application of the integral equation method to solve a variety of flow and acoustic problems. Due to the presence of the free surface it has taken some time before a straightforward application of this method in the field of ship waves has led to efficient computer codes. Since then the main emphasis in research seems to have shifted towards the development of numerical methods and fast computer codes. The skills to develop analytic models as a tool seem to have diminished. We are now in the stage that this trend of neglecting analytic skills reverses for several reasons. It can be that for special applications, for instance the wave resistance for extremely blunt bodies, one has to rely on the insight obtained by asymptotic expansions to decide what effects have to be taken into account acurately. In the case of linear wave diffraction by objects, at zero speed, the free surface Green's function needs many analytic manipulations to make it tractable computionally. On the other hand if one shifts to the time-domain and uses Rankine sources the problem arises that one likes to keep the computational domain as small as possible. One of the ways to force proper radiation can be done by a special formulation, where analytic manipulations play a role, of the outer region. The advantage of these methods is that one can shift to more general problems easely, the effects of forward speed or non-linear free surface effects can be taken into account. Analytic methods are also needed to analyse the properties of the numerical schemes, for instance numerical stability must be guaranteed, but also the effects of numerical dispersion may be of importance for certain applications.

In the following sections of this paper we will demonstrate the role of analytic methods in the development of these numerical algorithms. In the next section we consider the case of the still water resistance. Most of the presented material can be found in the doctor-thesis of Raven (1996). In the third section the zero speed harmonic case, as treated in the thesis of *Huijsmans* (1996), together with the unsteady moderate speed sea-keeping problem, related to the theses of *Prins* (1995) and *Sierevogel* (1998), are considered. The high Froude number sea-keeping work of *Bunnik* (1998) is a combination of methods derived by Raven, Prins and Sierevogel. In the fourth section the schemes are analysed with analytic methods.

2 Wave resistance

We restrict ourselves to the non-viscous part of the resistance felt by the ship at constant speed in still water. The flow is assumed to be irrotational. This means that we only consider the field around the ship that can be described by a steady potential field, where the steady velocity vector can be described as

$$\vec{V}(\vec{x}) = \nabla\Phi(\vec{x})$$

As a consequence of the incompressibility of the fluid the potential Φ fulfills the Laplace equation $\Delta\Phi(\vec{x}) = 0$. The pressure distribution in the fluid then follows by means of the stationary Bernoulli equation

$$\frac{p(\vec{x})}{\rho} + gz + \nabla\Phi \cdot \nabla\Phi = C$$

where C is a constant. The boundary conditions are given on the hull and the free surface. On the hull we have $\Phi_n = 0$, while at the free surface, $z = \zeta(x,y)$, the dynamic boundary condition reads $p(\vec{x}) = p_0$, the atmospheric pressure, and the kinematic condition $\Phi_n = 0$. Besides the conditions mentioned a far field condition for the disturbances has to be imposed. This so called radiation condition states that the disturbance is non-wavy far upstream. Downstream a wave-like behaviour must be present. The upstream condition reads

$$\Phi = Ux + O(\frac{1}{\sqrt{x^2+z^2}}) \quad \text{for } x \to -\infty$$

where U is the ship's speed.
The major difficulty in solving this boundary value problem stems from the highly non-linear free surface condition. The classical approximation of Michell consists of a linearization with respect to the unperturbed potential

$$\Phi(\vec{x}) = Ux + \phi(\vec{x})$$

The linearized free surface condition becomes

$$U^2\phi_{xx} + \phi_z = 0 \quad \text{at } z = 0 \tag{1}$$

This condition is only valid if one introduces a small parameter, for instance the beam/length ratio, and if the perturbation potential ϕ is small with respect to the unperturbed flow, uniformely. In this case, if the symmetric ship hull is defined as $y = f(x,z)$, the well known formula of Michell for the resistance reads,

$$R = \frac{4\rho g^2}{\pi U^2} \int_0^{\pi/2} \{\mathcal{P}^2(\theta) + \mathcal{Q}^2(\theta)\} \sec^3\theta \, \mathrm{d}\theta \tag{2}$$

where

$$\mathcal{P}(\theta) = \iint_H f_x(x,z) e^{\kappa z \sec^2\theta} \cos(\kappa x \sec\theta) \, \mathrm{d}x \, \mathrm{d}z$$

$$\mathcal{Q}(\theta) = \iint_H f_x(x,z) e^{\kappa z \sec^2\theta} \sin(\kappa x \sec\theta) \, \mathrm{d}x \, \mathrm{d}z$$

with the wave-number $\kappa = g/U^2$.
This result can be used for a wide range of hull forms, even for rather blunt bodies. In the latter case it is observed that the results become worse if one considers low Froude numbers. One may

say that the fact that the approximation of the potential is not uniformely valid, especially near the stagnation points, becomes apparent in the numerical results obtained by the Michell integral. Near the stagnation points the local wave-number is much smaller than the wave-number κ related to the unperturbed flow velocity U.

Due to the short wave length phenomenon at low speed some efforts are made to apply the ray method, well known in acoustic diffraction, but before doing so one has to decide about what free surface condition is essential in this region. Several authors have derived linearized free surface conditions applicable at low speed. Finally Eggers (1981) derived a condition that is asymptotically consistent, as shown by Hermans and Van Gemert (1989), later. In the doctor thesis of Brandsma (1987) an equivalent free surface condition is used and the ray method is successfully to obtain the wave pattern and an approximate of the wave resistance for bodies with a wedge-shaped bow and stern. The values of the resistance are well below the ones determined with Michell's formula. In this approach the potential is decomposed as a superposition of the 'double body' potential $\Phi_r(\vec{x})$ and a perturbation potential $\phi(\vec{x})$. This is intuitively a good approach, because at low speed the measured fluid velocity near the bow is very good approximated by the double body fluid velocity as was found by Baba (1976). Hermans and van Gemert (1989) have shown that this choice is the only correct one in the asymptotic theory. Hence, we write

$$\Phi(\vec{x}) = \Phi_r(\vec{x}) + \varphi(\vec{x}) \tag{3}$$

where $\Phi_r(\vec{x})$ fulfils the condition $\Phi_{rz}(\vec{x}) = 0$ at $z = 0$. If the potential function is determined we may compute the free surface elevation by means of the dynamic free surface condition. It will be clear that the '*double body potential*' leads to an elevation, $\zeta_r(x,y)$, just as well. So it is possible to transform the free surface condition for $\varphi(\vec{x})$ to this level. An easier way to do this is to introduce a new z-coordinate $z' = z - \zeta_r(x,y)$. This also influences the Laplace operator, but it can be shown that it only gives rise to lower order term with respect to the small Froude number. Discarding the accent we get the following linearized free surface condition,

$$\begin{aligned} \varphi_z &+ \frac{1}{g}[\Phi_{rx}^2\varphi_{xx} + 2\Phi_{rx}\Phi_{ry}\varphi_{xy} + \Phi_{ry}^2\varphi_{yy}] \\ &+ (3\Phi_{rx}\Phi_{rxx} + 2\Phi_{ry}\Phi_{rxy} + \Phi_{rx}\Phi_{ryy})\varphi_x + \\ &+ (3\Phi_{ry}\Phi_{ryy} + 2\Phi_{rx}\Phi_{rxy} + \Phi_{ry}\Phi_{rxx})\varphi_y = \mathcal{D}(x,y) \qquad \text{at } z = 0 \end{aligned} \tag{4}$$

where the function $\mathcal{D}(x,y)$ only depends on Φ_r

$$\mathcal{D}(x,y) = \frac{\partial}{\partial x}[\Phi_{rx}(x,y,0)\zeta_r(x,y)] + \frac{\partial}{\partial y}[\Phi_{ry}(x,y,0)\zeta_r(x,y)] \tag{5}$$

Expansion of (4) with respect to the $z = 0$ in the original coordinate system leads to the linearized free surface condition of Eggers.

Based on this free surface condition Brandsma (1986) applied the asymptotic ray method. Assuming for large values of the wave-number $\kappa = \frac{g}{U^2}$ a far-field solution of the form,

$$\varphi(\vec{x}) = \Re\left[\left(\frac{U}{i\kappa}a_0(\vec{x}) + \frac{U}{(i\kappa)^2 L}a_1(\vec{x}) + \cdots\right)\exp\left(i\kappa S(\vec{x})\right)\right], \tag{6}$$

one may obtain at the free surface for the phase function $S(x,y)$ and the first term of the expansion of the amplitude function $a_0(x,y)$ the eikonal of the form:

$$(MS)^4 - \left(\frac{\partial S}{\partial x}\right)^2 - \left(\frac{\partial S}{\partial y}\right)^2 = 0 \quad \text{at } z = 0, \tag{7}$$

where the differential operator M is given as

$$M = \frac{1}{U}\left(\Phi_{rx}(x,y,0)\frac{\partial}{\partial x} + \Phi_{ry}(x,y,0)\frac{\partial}{\partial y}\right),$$

and along the characteristics of this eikonal equation the transport equation of the form

$$\frac{\mathrm{d}a_0}{\mathrm{d}x} = f(x)a_0 \tag{8}$$

with

$$f(x) = \frac{-\frac{1}{2}(MS)^{-2}\Delta S + M^2 S - \nabla\overline{\zeta}_r \cdot \nabla S - \frac{\Phi_{rzz}}{U} MS}{2MS\Phi_{rx} - (MS)^{-2}S_x}.$$

This approach may be applied to simplified ship forms, in those cases one may show that main contribution to the wave-pattern is generated at the bow and the stern and expressions may be obtained for the excitation coefficients needed as initial conditions for the transport equation. The ray patterns for a lens-shaped body with bow and stern angle equal $\beta_b = \pi/8$ are shown in figure (1).

The wave resistance is computed with the help of the far field expansion.

$$\mathcal{R}_w = \frac{1}{2}\rho\pi U^2 \int_{-\pi/2}^{+\pi/2} |A(\theta)|^2 \cos^3\theta \,\mathrm{d}\theta \tag{9}$$

where $A(\theta)$ is the free wave spectrum in the far field behind the ship. This formulation of the wave resistance follows from conservation of momentum around the ship. Numerical results for the the wave resistance are shown in figure (2). This method gives some insight in the phenomena that are of importance but, due to the severe geometrical limitations, it is not appicable for general hull forms.

Dawson (1977) suggested a direct numerical approach. The potential is written as a superposition of the double body and a perturbation potential as in (3). He uses a simplified free surface condition consisting of derivatives along the stream lines of the double body potential.

$$(\Phi_{rl}^2 \varphi_l)_l + \varphi_z = 2\Phi_{rl}^2 \Phi_{rll} \quad \text{at } z = 0 \tag{10}$$

The boundary value problem is solved by means of a distribution of Rankine sources along the free surface and the ship hull. The velocity components at the free surface expressed, as integrals over the distributions of the unknown source strength, are obtained by differentiation. The latter expressions are differentiated by means of a finite difference operator to express the second

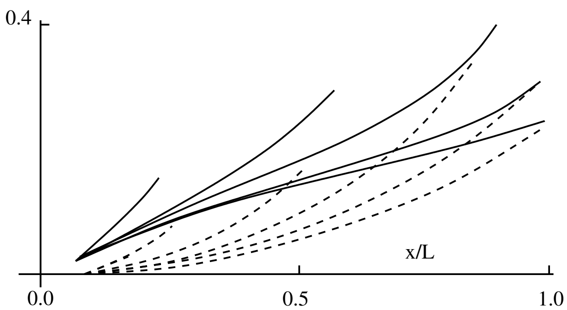

Figure 1: Some wave-fronts for the diverging bow-wave system $\beta_b = \pi/8$, ___ non-linear results and _ _ _ _ linear results.

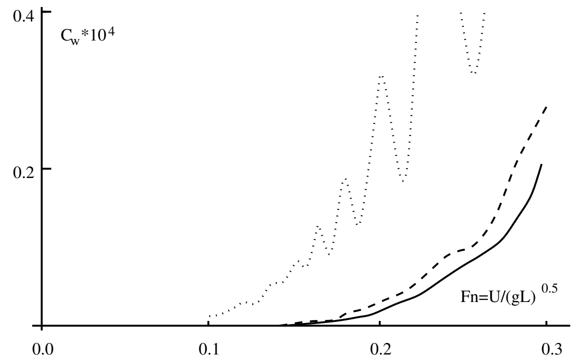

Figure 2: Comparison of $C_w = \frac{R_w}{\frac{1}{2}\rho U^2 L^2}$ for $\beta_b = 0.1974$, $\cdots\cdots$ Michell, _ _ _ _ Baba, ___ present theory.

order derivatives of the potential function in the unknown source strengths. The integrals are discretized by a panel method. Because the free surface condition expresses the z-derivative of the potential in derivatives of the velocity component along the stream-lines one may write these derivatives by a finite difference scheme easely if a stream-line paneling is chosen. The radiation condition indicates that an upwind finite difference operator may be a good choice. This turned out to be a good choice. Several authors have improved this concept of Dawson and finally it is the basis of many well tested solvers. The codes are used for many practical case in an early stage of the design of ships. An overview of its applicabillity can be found in Raven (1996).

Despite its success there are several shortcoming of the Dawson approach. For instance for blunt ships at low forward speed the pressure integration along the hull may render values of the wave resistance that are not close to the measurements systematically. The computed values sometimes are negative. Refinement of the mesh shows that in those cases one finds convergence to this erroneous value, while the wavy pattern along the hull looks very realistic. The first suggestion was to make the linearized free surface more realistic. Raven considered the influence of several terms in the free surface condition. For instance he studied effect the transfer terms, not taken into account in (10), and he also replaced (10) by (4). The latter is the most complete linearized free surface condition. In several cases the wave pattern becomes better than the ones obtained originally, however, the computations of the wave resistance remains inaccurate or even negative. This was the main reason for the development of a fully non-linear code. The resulting RAPID (RAised Panel Iterative Dawson) code improved both the wave profile and the values of the wave resistance for a broad class of ships. In both the Dawson and the RAPID code a transom stern can be taken into account. This necessitates some extra mathematical modelling of the local flow.

The question remains whether a mathematical analysis of the underlying concepts may improve the approach. For instance, numerical experiments have shown that the choice of the collocation point and the distance of the raised panels to the physical surface are crucial for the performance of the scheme. For this purpose an accuracy analysis may be carried out. For the final formulation this may result in a heavy computational excercise. However, the analysis of a simple case sometimes gives sufficient information. Raven (1996) analysed the effect of several choices in his method by applying his analysis to the 2D case with the simplified Kelvin free surface condition (1). In the next section it will turn out that in our approach to solve the sea keeping problem a similar analysis is needed for the choice of an appropriate scheme, hence, we address this analysis in section 4.

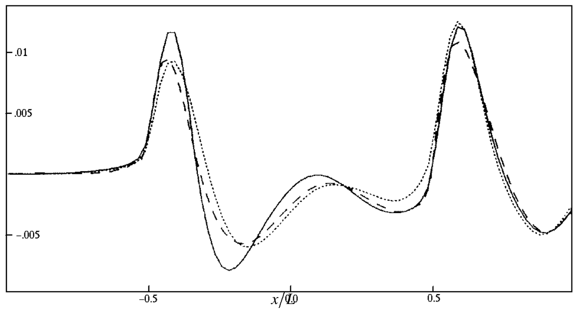

Figure 3: Hull wave profile (ζ/L) predictions, Wigley hull, $Fn = 0.316$, ·· Kelvin, —— RAPID, − − DAWSON

Results

Here we have selected some of the results obtained by Raven (1966). In his study a variety of hull forms is discussed. We restrict ourselves to a Wigley hull and a Series 60 hull. Details of the particular hull forms can be found in Raven (1996). In figure 3 the effect of different methods in the calculation of the wave profile along a Wigley hull at $F_n = 0.316$. For this unusual slender hull ($L/B = 10$) it is apparent that nonlinear effects are significant. It is found that the profile obtained with the nonlinear agrees with the wave profile measured in the ITTC Cooperative Experimental Program. The only exception is the height of the bow wave, which is on a very fine grid about 11% less than in the experiment. This deviation could be due to spray, which makes an experimental bow wave determination rather uncertain, but it is likely that it at least partly has to do with incomplete resolution of the singular behaviour at the bow. The effect seems to be quite localised.

For the Series 60 Cb=0.60 model longitudinal and transverse wave cuts are measured ($F_n = 0.316$) at the Iowa Institute of Hydraulic research. Figure 4 shows the nonlinear and linearized predictions for some longitudinal cuts. The differences are small in this case, but the nonlinear result is consistently the best. Both linearized methods slightly underestimate most wave amplitudes; the Kelvin results in addition has a phase lag at a distance from the hull. Only the nonlinear results seem to include all high-wavenumber contributions. Figure 5 compares the predicted wave resistance with some experimental data (Iowa Inst.) for the residual resistance. While the agreement is excellent, it must be noticed that for this case experimental results from various tanks appeared to have a substantial scatter. Moreover, the predictions actually seem to be on the high side; no form factor has been used to estimate the viscous resistance, so the vis-

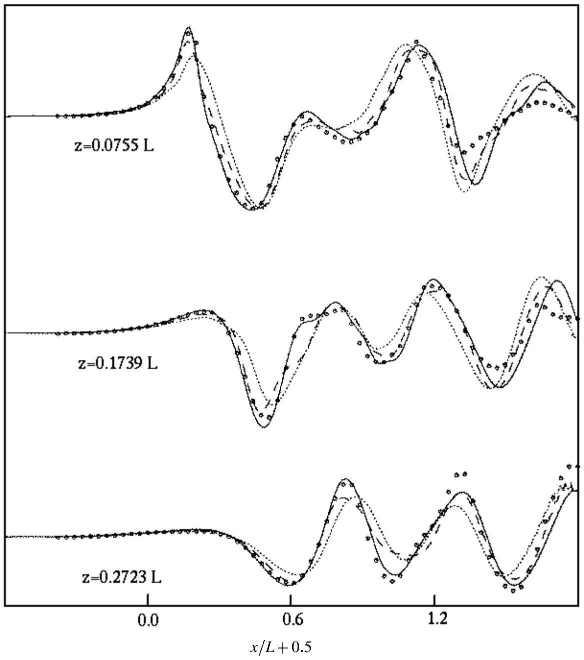

Figure 4: Longitudinal wave cuts for Series 60 model, $Fn = 0.316$

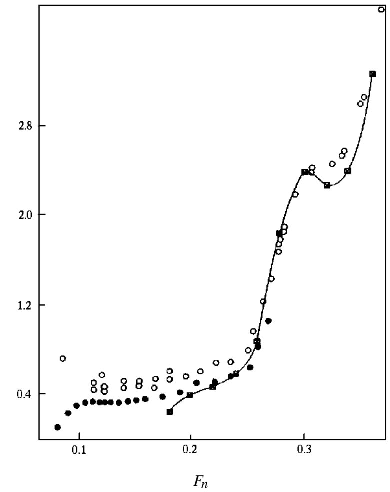

Figure 5: Predicted wave resistance and experimental residual resistance coefficients ($C_w \times 100$), free trim and sinkage

cous drag is included in the residual resistance data. Anyway, the shape of the resistance curve is quite accurately reproduced.

3 Potential theory for ship motions

In literature a variety of methods to compute the first order potentials can be found. For zero forward speed the most commonly used method is based on the application of Green's theorem to the fluid domain, or based on a source distribution, using the harmonic Green's function, which obeys the linearised free surface condition. Some computer codes are commercially available, they treat both the infinite depth or the finite depth case. Newman (1985,1992) and Noblesse (1982), independently, made ingeneous fast codes to compute the Green's function and its derivatives. The sources of the codes are either commercially or freely available. The panel method codes developed with these source functions vary widely from zero order (constant) to higher order methods, there are also codes making use of spline approximations.

Meanwhile codes are developed that make use of simple Rankine, $\frac{1}{r}$ sources, so they consist of source distributions over the object and the free surface, one of the first successful efforts can be found in the work of Yeung (1973). This can be done in the frequency-domain or in the time-domain. The linearised versions consider the free surface source distribution along $z = 0$, while the nonlinear versions may have a distribution at the actual free surface. In the latter case the free surface is determined iteratively. Also, the source strength on a panel can be described by lower or higher order appoximations.

To compute the diffraction of waves in a current or by a steadily moving object there is a Green's function available that obeys the linearized free surface condition for harmonic waves in a uniformly constant flow. Some attemps to use this Green's function in a similar code as described above did not give a substantional improvement of the results obtained by the classical widely available strip-theory. This strip-theory, in principle, makes use of the slenderness or thinness. Hence, the the stationary potential is approximated by the unperturbed flow. This theory leads to an approach that is two-dimensional, sideways, in nature. Three-dimensional effect are taking into account by means of the interaction of adjacent strips. The modified strip theory gives rather accurate results for a large class of ships. However in the case of full bodied ships and offshore structures in current this appraoch is not reliable. The frequency-domain and time-domain methods based on a superposition of the double body potential and the wave potential may lead to a significant improvement.

In the next subsections we discuss two different ways to compute the first order diffraction and radiation potential superimposed on the double body potential. These approaches are suitable for low to moderate forward velocity or current. At high speed it is expected that these methods have to be improved, see Bunnik(1998).

3.1 Slow speed approximation

We first derive the equations for the potential function $\Phi(\vec{x},t)$, such that the fluid velocity $\vec{u}(\vec{x},t)$ is defined as $\vec{u}(\vec{x},t) = \nabla\Phi(\vec{x},t)$. The total potential function will be split up in a steady and a non-steady part in a well-known way:

$$\Phi(\vec{x},t) = Ux + \bar{\phi}(\vec{x};U) + \tilde{\phi}(\vec{x},t;U)$$

In this formulation U is the incoming unperturbed velocity field, obtained by considering a coordinate system fixed to the ship moving. The time dependent part of the potential consists of an incoming, diffracted and radiated (for six modes of motion) wave

$$\tilde{\phi}(\vec{x},t;U) = \tilde{\phi}^{inc}(\vec{x},t;U) + \tilde{\phi}^{(7)}(\vec{x},t;U) + \sum_{i=1}^{6} \tilde{\phi}^{(i)}(\vec{x},t;U)$$

at frequency $\omega = \omega_0 + k_0 U \cos\beta$, where ω_0 and $k_0 = \omega_0^2/g$ are the frequency and wave number in the earth fixed coordinate system, while ω is the frequency in the coordinate system fixed to the ship. The waves are incident under an angle β, with respect to the current. To compute the wave drift forces all these components will be taken into account.
The equations for the total potential Φ can be written as:

$$\Delta\Phi = 0 \text{ in the fluid domain } D_e$$

At the free surface we have the dynamic and kinematic boundary condition:

$$\left.\begin{array}{r} g\zeta+\Phi_t+\frac{1}{2}\nabla\Phi\cdot\nabla\Phi=\mathcal{C}_{st} \\ \Phi_z-\Phi_x\zeta_x-\Phi_y\zeta_y-\zeta_t=0 \end{array}\right\} \text{ at } z=\zeta \tag{11}$$

At the body surface we have:

$$\frac{\partial\Phi}{\partial n}=\vec{V}\cdot\vec{n}$$

where $\vec{V}$ is the body velocity relative to the average body fixed coordinate system.
We assume that the waves are high compared to the Kelvin stationary wave pattern, but that they are both small in nature, hence the free surface boundary condition can be expanded at $z=0$. We first eliminate ζ, this leads to the following boundary condition:

$$\frac{\partial^2}{\partial t^2}\Phi+g\frac{\partial}{\partial z}\Phi+\frac{\partial}{\partial t}(\nabla\Phi\cdot\nabla\Phi)+\frac{1}{2}\nabla\Phi\cdot\nabla[\nabla\Phi\cdot\nabla\Phi]=0 \text{ at } z=\zeta \tag{12}$$

To compute the first order wave potential the free surface has to be linearized first. We assume $\tilde{\phi}(\vec{x},t;U)=\phi(\vec{x};U)\exp(-i\omega t)$, then for $i=1,\ldots,6$ the free surface condition at $z=0$ can be written as:

$$-\omega^2\phi-2i\omega U\phi_x+U^2\phi_{xx}+g\phi_z=\mathcal{D}(U;\overline{\phi})\{\phi\} \text{ at } z=0 \tag{13}$$

while for the diffracted potential $\phi^{(7)}$ the last term has to be repalced by $\mathcal{D}(U;\overline{\phi})\{\phi^{inc}+\phi^{(7)}\}$ and where $\mathcal{D}(U;\overline{\phi})$ is the following linear differential operator acting on ϕ. The quadratic terms in ϕ are neglected.

$$\begin{aligned}\mathcal{D}(U;\overline{\phi})\{\phi\} &= -i\omega\{(\overline{\phi}_{xx}+\overline{\phi}_{yy})\phi+2\nabla\overline{\phi}\cdot\nabla\phi\} \\ &\quad +(2U\overline{\phi}_x+\overline{\phi}_x^2)\phi_{xx}+2(U+\overline{\phi}_x)\overline{\phi}_y\phi_{xy}+\overline{\phi}_y^2\phi_{yy} \\ &\quad +(3U\overline{\phi}_{xx}+\overline{\phi}_x\overline{\phi}_{xx}+\overline{\phi}_y\overline{\phi}_{xy})\phi_x+(2U\overline{\phi}_{xy}+\overline{\phi}_x\overline{\phi}_{xy}+\overline{\phi}_y\overline{\phi}_{yy})\phi_y\end{aligned}$$

The linear problems for $\phi^{(i)}$ with $i=1,\ldots,7$ are solved by means of a source distribution along the ship hull, its waterline and the free surface $z=0$. We write for each potential function:

$$\begin{aligned}4\pi\phi(\vec{x}) = &-\iint_S\sigma(\vec{\xi})G(\vec{x},\vec{\xi})\,\mathrm{d}S_\xi+\frac{U^2}{g}\int_{WL}\alpha_n\sigma(\vec{\xi})G(\vec{x},\vec{\xi})\,\mathrm{d}s_\xi \\ &+\frac{i\omega}{g}\iint_{FS}G(\vec{x},\vec{\xi})\mathcal{D}\{\phi\}\,\mathrm{d}S_\xi \qquad \text{for } \vec{x}\in D_e\end{aligned} \tag{14}$$

The function $G(\vec{x},\vec{\xi})$ is the Green's function that obeys the free surface condition (13) with $\mathcal{D}$ equals zero and $\alpha_n=\vec{e}_x\cdot\vec{n}$, where $\vec{e}_x$ equals the unit vector in the x-direction. In general the boundary conditions on the ship are given in the form:

$$\nabla\phi^{(j)}\cdot\vec{n}=V^{(j)}(\vec{x}) \quad \text{for } \vec{x}\in S \text{ and } j=1,\ldots,7$$

where $V^{(j)}$ is the normal velocity due to the motion in the j'th mode with $j=1,\ldots,6$ and $V^{(7)}$ equals the normal velocity of the incident oscillating field. So $V^{(j)}$, with $j=1,\ldots,3$, correspond to the translation components $\vec{X} = \vec{\tilde{X}} \exp(-i\omega t)$ and, with $j = 4, \ldots, 6$, to components of the rotational motion $\vec{\Omega} = \vec{\tilde{\Omega}} \exp(-i\omega t)$ relative to the centre of gravity $\vec{x}_g$ of the body. The combined displacement vector is given by $\vec{\alpha} = \vec{X} + \vec{\Omega} \times (\vec{x} - \vec{x}_g) = \vec{\tilde{\alpha}} \exp(-i\omega t)$. In general notation we write

$$\frac{\partial\phi}{\partial n} = -i\omega\vec{\tilde{\alpha}} \cdot \vec{n} + [(\nabla(Ux + \overline{\phi}) \cdot \nabla)\vec{\tilde{\alpha}} - (\vec{\tilde{\alpha}} \cdot \nabla)\nabla(Ux + \overline{\phi})] \cdot \vec{n}$$

This leads to an equation for the source strength, where we omitted the index i again:

$$\begin{aligned} -2\pi\sigma(\vec{x}) - \iint_S \sigma(\vec{\xi}) \frac{\partial}{\partial \vec{n}_x} G(\vec{x}, \vec{\xi}) \, \mathrm{d}S_\xi + \frac{U^2}{g} \int_{WL} \alpha_n \sigma(\vec{\xi}) \frac{\partial}{\partial \vec{n}_x} G(\vec{x}, \vec{\xi}) \, \mathrm{d}s_\xi \\ + \frac{i\omega}{g} \iint_{FS} \frac{\partial}{\partial \vec{n}_x} G(\vec{x}, \vec{\xi}) \mathcal{D}\{\phi\} \, \mathrm{d}S_\xi = 4\pi V(\vec{x}) \quad \text{for } \vec{x} \in S \end{aligned} \tag{15}$$

This equation can be solved iteratively in principle, however an accurate numerical evaluation of the complete Green's function is rather elaborate. Therefore we make use of the fact that U is small, keeping in mind that there are two dimensionless parameters that play a role, namely $\tau = \frac{\omega U}{g} \ll 1$ and $\nu = \frac{gL}{U^2} \gg 1$. The source potentials and the strengths can be evaluated as perturbation series with respect to τ

$$\sigma(\vec{\xi}) = \sigma_0(\vec{\xi}) + \tau\sigma_1(\vec{\xi}) + \hat{\sigma}(\vec{\xi}; U) \tag{16}$$

$$\phi(\vec{x}) = \phi_0(\vec{x}) + \tau\phi_1(\vec{x}) + \hat{\phi}(\vec{x}; U) \tag{17}$$

where $\hat{\sigma}$ and $\hat{\phi}$ are $O(\tau^2)$ as $\tau \to 0$, while the expansion of G is less trivial. We write:

$$\begin{aligned} G(\vec{x}, \vec{\xi}; U) = -\frac{1}{r} + \frac{1}{r'} - \{\psi_0(\vec{x}, \vec{\xi}) + \tau\psi_1(\vec{x}, \vec{\xi}) + \cdots \\ \cdots \tilde{\psi}_0(\vec{x}, \vec{\xi}) + \nu^{-1}\tilde{\psi}_1(\vec{x}, \vec{\xi}) + \cdots\} \end{aligned} \tag{18}$$

The first term between brackets corresponds to the Green's function at zero forward speed, for which there exist several fast computer codes. The second term is the modification due to small values of the forward velocity. Computations can be carried out by means of a modification of the existing fast code. Nonuniformities can be taken care of as described by Huijsmans (1996). The third term between brackets is the one that describes the Kelvin effect on the wave Green's function. Hermans (1987) explains how one takes care of this term that is linear in ν and therefore tends to infinity as U goes to zero. In practice the first two terms are computed in the expansions of the potentials and the source strengths for the excitation and the six modes of the motion. This approach is easily applied to the situation of deep water. For finite water depth the evaluation of the Green's function for finite velocities leads to terms that are not as easy to compute as in the deep water case, where all the expressions needed can be expressed in derivatives of the zero speed Green's function.

3.2 Time-domain simulation

Recently Prins (1995) and Sierevogel (1998) developed a time-domain method to compute the first order time dependent part of the potential function. With this approach the complete potential function is written as follows:

$$\Phi(\vec{x},t) = \overline{\Phi}(\vec{x}) + \psi(\vec{x},t)$$

For small values of the forward velocity the stationary potential $\overline{\Phi}(\vec{x})$ is approximated by the double-body potential with zero vertical velocity at the mean free surface $z = 0$. We insert this expression in 12 and linearise the resulting expression at $z = 0$, we obtain:

$$\frac{\partial^2\psi}{\partial t^2} + g\frac{\partial\psi}{\partial z} + 2\nabla\overline{\Phi}\cdot\nabla\frac{\partial\psi}{\partial t} + \frac{1}{2}\nabla(\nabla\overline{\Phi}\cdot\nabla\overline{\Phi})\cdot\nabla\psi + \nabla\overline{\Phi}\cdot\nabla(\nabla\overline{\Phi}\cdot\nabla\psi) -$$
$$\frac{1}{2}(\nabla\overline{\Phi}\cdot\nabla\overline{\Phi} - U^2)\left(\frac{\partial^2\psi}{\partial z^2} + \frac{1}{g}\frac{\partial^3\psi}{\partial t^2\partial z}\right) - \frac{\partial^2\overline{\Phi}}{\partial z^2}\left(\nabla\overline{\Phi}\cdot\nabla\psi + \frac{\partial\psi}{\partial t}\right) = 0 \text{ at } z = 0 \tag{19}$$

The solution method is based on the applications of Green's theorem for the fluid domain. For $x \in \partial V$ we write:

$$\frac{1}{2}\psi(\vec{x},t) = \int_{\partial V}\left(\psi(\vec{\xi},t)\frac{\partial G(\vec{x},\vec{\xi})}{\partial n_\xi} - \frac{\partial\psi(\vec{\xi},t)}{\partial n_\xi}G(\vec{x},\vec{\xi})\right)\,\mathrm{d}S \tag{20}$$

In this formulation the Green's function is chosen as the point-source at $\vec{x} = \vec{\xi}$ obeying the bottom condition, hence

$$G(\vec{x},\vec{\xi}) = \frac{1}{4\pi}\left(\frac{1}{|\vec{x}-\vec{\xi}|} + \frac{1}{|\vec{x}-\vec{\xi}^*|}\right)$$

where $|\vec{x}-\vec{\xi}^*|$ is the distance to the source point reflected with respect to the flat bottom at $z = -h$. The integration is taken over the object, the free surface $z = 0$ and the outer closing boundaries. If one assumes the time-dependent potential to be a superposition of the nondisturbed incident wave, the diffracted wave potential and the radiation (motion) potential one can compute the diffracted or the radiated by imposing the free surface condition and the body boundary condition. The closing boundaries need some extra care, one should impose a proper non-reflecting boundary condition. The differentiations along the free surface are handled by means of a central or upwind difference scheme, while the time differentiation is treated with an implicit difference scheme. In the next section we give the analysis of the consequences of the choice of the kind of scheme, to be chosen. In principle, we want to be able to compute the disturbance due to a general non-harmonic incident wave. We also want to keep the computing area as small as possible. This makes the choice of the non-reflecting boundary condition at the outer boundaries non trivial. For harmonic waves and the boundaries far away we may choose a Sommerfeld type of condition, taking care of the two families of waves in the uniform current time harmonic case. This has been done by Prins (1995). Sierevogel (1998) implemented a formulation for the general case. Several efficient methods are available, the method we implied is of the class of semi-discrete DtN-method, see Keller and Givoli (1989). The number of unknowns in the equations is increased by a small amount namely the amount of elements at the outer boundaries. This approach is very efficient, it leads to a minor increase of computation time. The outer boundaries can be chosen at a rather small distance, depending on the wavelength and the steady velocity disturbance. An extensive study of non-reflecting boundary conditions for the acoustic case can be found in the book of Givoli (1992).

The time-derivatives at the free surface is written by means of an explicit difference scheme at $t = (n+1)\Delta t$ as follows:

$$\psi_z^{n+1} + \mu\psi^{n+1} = \mu\mathcal{L}(\psi^n, \psi^{n-1}, \cdots) \tag{21}$$

where $\mu = \frac{2}{g(\Delta t)^2}$ and $\mathcal{L}(\psi^n, \psi^{n-1}, \cdots)$ is a linear operator depending on previous time steps only. If one takes the outer domain far enough, such that the steady potential can be approximated by the undisturbed flow Ux the right hand side can be written, for a second order difference scheme, as

$$\begin{aligned}\mathcal{L}(\psi^n, \psi^{n-1}, \cdots) &= 5\psi^n - 4\psi^{n-1} + \psi^{n-2} - \frac{U\Delta t}{2}(5\psi_x^n - 8\psi_x^{n-1} + 3\psi_x^{n-2}) \\ &- \frac{(U\Delta t)^2}{2}(3\psi_{xx}^n - 3\psi_{xx}^{n-1} + \psi_{xx}^{n-2})\end{aligned}$$

If the far field approximation of the steady field is not accurate enough in the right hand side also terms with the perturbed steady potential are involved. Furthermore the method is based on a the application of Green's theorem to the exterior domain. The Green's function obeys the field equations, bottom condition and the homogeneous free surface condition. In the deep water case it has the form,

$$4\pi G(\vec{x}, \vec{\xi}) = -\frac{1}{r} - \int_0^\infty \frac{k-\mu}{k+\mu}\, \mathrm{e}^{kZ} J_0(kX)\, \mathrm{d}k \tag{22}$$

where X is the horizontal distance, $X^2 = (x-\xi)^2 + (y-\zeta)^2$ and $Z = z + \zeta$. If one compares this formula with the ordinary *'wavy'* Green's function, see Wehausen and Laitone (1960) one notices that the only difference is the sign in front of the parameter μ, this was already visible in the formulation of the discretized free surface condition. The fact that the integrand of (22) does not have a pole on the real k axis makes it easy to compute. It can be rewritten in analogy with Noblesse (1982) as follows

$$4\pi G(\vec{x}, \vec{\xi}) = -\frac{1}{r} - \frac{1}{r_1} + 2\int_0^\infty \frac{\mathrm{e}^{-k}}{\sqrt{\frac{k}{\mu} - Z)^2 + X^2}}\, \mathrm{d}k \tag{23}$$

The integral can be computed passable quickly, using fast Gauss-Laguerre integration routines, which integrate funsions written as $\int_0^\infty e^{-x} f(x)\, \mathrm{d}x$. If one integrates over the panel at the free surface first and then with respect to k the panel can be taken rather large to obtain sufficient accuracy. This operation has to be done once, because each time step a matrix vector multiplication takes care of the known right-hand side, also obtained by matrix vector multiplication, of the free surface condition. In the finite water depth case this procedure can be carried out, just as well. Details can be found in Sierevogel (1998).

4 Analysis of the difference schemes

The choice of the difference scheme for the derivetives at the free surface influence the performance of the codes heavily. Nakos (1990), Raven (1996), Sierevogel (1998) and Bunnik (1998) applied comparable analyses to their particular schemes. We will follow the analysis of Sierevogel and at the end show results of Raven as well.

Inaccuracies appear when the numerical actual wavelength differs from the actual one, this difference is called dispersion, or when the wave amplitude decreases or increases, this is called damping or amplification. Instabilities apear when the wave amplitude increases rapidly. These inaccuracies and instabilities depend on the discretization of the time and space, thus on the panel size and time step, or on the order of the difference scheme, for instance. The increase in the forward speed in section 3.2 causes numerical instabilities if at the free surafce a central difference scheme is chosen. If one chooses an upwind scheme in the direction of the streamlines of the steady flow they disappear. In the sequel we will show how the schemes can be analysed, such that a proper choice can be made.

For simplicity, this analysis is restricted to a 2D test problem and the steady potential is approximated by the unperturbed flow potential Ux. Bunnik (1998) extended this approach to the 3D case. The linearized free surface condition (19) reduces to

$$g\psi_z = -\psi_{tt} - 2U\psi_{xt} - U^2\psi_{xx} \text{ at } z = 0 \tag{24}$$

At the free surface $z = 0$ we express the value of the potential function $\psi(\vec{x},t)$ in terms at the free surface and an integral at the body in a suitable way for the acuracy analysis. Making use of (24) the Green theorem leads to

$$\frac{1}{2}\psi(x,0,t) - \frac{1}{g}\int_{\mathcal{F}}\left(\frac{\partial^2}{\partial t^2} + 2U\frac{\partial^2}{\partial\xi\partial t} + U^2\frac{\partial^2}{\partial\xi^2}\right)\psi(\xi,0,t)G(x-\xi)\,\mathrm{d}\xi = RHS \tag{25}$$

with the right hand side, rewritten formally as a convolution

$$RHS = \int_{\partial S\backslash f}\left(\psi G_{n\xi} - G\psi_{n\xi}\right)\,\mathrm{d}\Gamma := \int_{\mathcal{F}} f(\xi,t)G(x-\xi)\,\mathrm{d}\xi \tag{26}$$

where f shall be formulated later on. The Green's function in this formulation is the simple source function $\frac{1}{2\pi}\log r$. Formally we rewrite equation (25) with the 'free-surface operator' $\mathcal{W}$ as

$$\mathcal{W}(x,t)\psi(x,t) = f(x,t) \tag{27}$$

where we shortened the notation for $\psi(x,0,t)$. The right hand side contains all integrals over the remainder of the boundary, as the body surface and the bottom. The error analysis is carried out in the Fourier space. We introduce

$$\widetilde{\psi}(k,\omega) = \int_{-\infty}^{\infty}\int_{-\infty}^{\infty}\psi(x,t)\;\mathrm{e}^{-i(\omega t-kx)}\,\mathrm{d}x\,\mathrm{d}t$$

and

$$\psi(x,t) = \frac{1}{(2\pi)^2}\int_{-\infty}^{\infty}\int_{-\infty}^{\infty} \widetilde{\psi}(k,\omega)\, \mathrm{e}^{i(\omega t-kx)}\, \mathrm{d}k\, \mathrm{d}\omega$$

with k the Fourier wave number in the x-direction and ω in the t-direction.

The Fourier transform for the Green's funtion at the free surface becomes

$$\widetilde{G}(k) = -\frac{1}{2|k|}$$

Application of the Fourier transform to (25) leads to

$$\left(\frac{1}{2}+\frac{1}{g}\left(\omega^2-2U\omega k+U^2k^2\right)\widetilde{G}(k)\right)\widetilde{\psi}(k,\omega) = \widetilde{RHS}(k,\omega) \tag{28}$$

It is convenient to define as transform of f in (26)

$$\widetilde{F}(k,\omega) = \frac{\widetilde{RHS}(k,\omega)}{\widetilde{G}(k)}$$

Transforming the solution at the free surface back into the physical space, leads to

$$\psi(x,t) = \frac{1}{4\pi^2}\int_{-\infty}^{\infty}\int_{-\infty}^{\infty} \frac{\widetilde{F}(k,\omega)}{\widetilde{\mathcal{W}}(k,\omega)}\, \mathrm{e}^{i(\omega t-kx)}\, \mathrm{d}\omega\, \mathrm{d}k \tag{29}$$

The dispersion relation for the continuous non-zero speed case becomes,

$$\widetilde{\mathcal{W}}(k,\omega) = -|k| + \frac{1}{g}(\omega^2-2U\omega k+U^2k^2) = 0 \tag{30}$$

and gives the following wave number for respectively $k>0$ and $k<0$

$$k = \frac{g+2U\omega \pm g\sqrt{1+\frac{4U\omega}{g}}}{2U^2} \quad \text{and} \quad k = \frac{-g+2U\omega \pm g\sqrt{1-\frac{4U\omega}{g}}}{2U^2}$$

These wave numbers with the smallest absolute value are represented graphically in fig 6, they will be compared with the ones resulting after applying panelisation of the integral and discretisation of the differentations. The solution $\psi(x,z,t)$ is discretized over a free-surface grid of uniform spacing Δx in the x-direction. In this case we choose the collocation points in the centre of the panel. The solution $\psi(x,z,t)$ is also discretized in time using a uniform step Δt. The discrete form of (25) becomes as follows

$$\frac{1}{2}\psi(x_i,t_n) - \frac{1}{g}\sum_{j=-\infty}^{\infty}\left(\frac{\partial^2}{\partial t^2}+2U\frac{\partial^2}{\partial \xi_j \partial t}+U^2\frac{\partial^2}{\partial \xi_j^2}\right)\psi(\xi_j,t_n)G_{\Delta x} = RHS \tag{31}$$

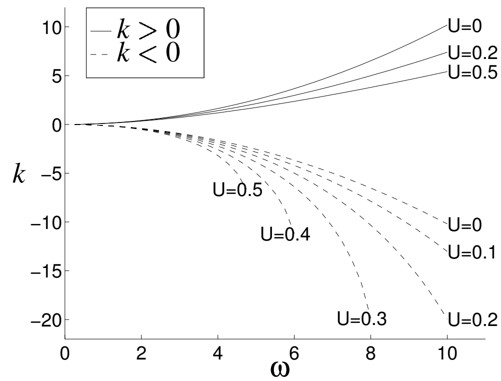

Figure 6: The wave number as function of the wave frequency, computed with the continuous dispersion relation. For $k > 0$ the wave number with minus the root is given, and for $k < 0$ the wave number with plus the root is given. The other wave numbers approaches g/U^2, and therefore become very large. The short waves belonging to these wave length do not exist in our problem, because of the panel size.

where the integral of the Green function over the panel is

$$G_{\Delta x} = G_{\Delta x}(x_i - \xi_j) = \int_{\xi_j - \frac{\Delta x}{2}}^{\xi_j + \frac{\Delta x}{2}} G(x_i - \xi)\, \mathrm{d}\xi$$

We shall now introduce the discrete Fourier tansform with respect to the x and t-coordinate as

$$\widehat{\psi}(k,\omega) = \Delta x \Delta t \sum_{m=-\infty}^{+\infty} \sum_{n=-\infty}^{+\infty} \psi(x_m, t_n)\, \mathrm{e}^{-i(\omega n \Delta t - k m \Delta x)}$$

and

$$\psi(x_m, t_n) = \frac{1}{4\pi^2} \int_{-\frac{\pi}{\Delta x}}^{+\frac{\pi}{\Delta x}} \mathrm{d}k \int_{-\frac{\pi}{\Delta t}}^{+\frac{\pi}{\Delta t}} \mathrm{d}\omega\, \widehat{\psi}(k,\omega)\, \mathrm{e}^{i(\omega n \Delta t - k m \Delta x}$$

where $x_m = m\Delta x$ and $t_n = n\Delta t$. The discrete convolution theorem states,

$$\text{if } a_m = \sum_{m=-\infty}^{+\infty} b_n c_{m-n} \text{ then } \widehat{a} = \frac{1}{\Delta x} \widehat{b}\widehat{c}$$

The semi-discrete Fourier transform of $G_{\Delta x}(x_m)$ becomes after some arithmetic

$$\widehat{G}(k) = -\sin(\widehat{k}\pi) \frac{1}{k^2}(1 - \varepsilon(\widehat{k})), \text{ with } \varepsilon(\widehat{k}) = \sum_{m=1}^{+\infty} \frac{4\widehat{k}^3}{m^3 \left(1 - \frac{\widehat{k}^2}{m^2}\right)^2}$$

where we have introduced the dimensionless parameter, $\widehat{k} = k\Delta x/(2\pi)$, the number of steps per wavelength. The serie expansion for $\varepsilon(\widehat{k})$ converges very quickly.

We apply the discrete Fourier transform to equation (31) and obtain

$$\left[\frac{\Delta x}{2\widehat{G}} - \frac{1}{g}\left(\frac{1}{(\Delta t)^2}\widehat{\mathcal{D}}^{(tt)} + \frac{U}{2\Delta x \Delta t}\widehat{\mathcal{D}}^{(t)}\widehat{\mathcal{D}}^{(x)} + \frac{U^2}{(\Delta x)^2}\widehat{\mathcal{D}}^{(xx)}\right)\right]\widehat{\psi} = \frac{\Delta x}{\widehat{G}}\widehat{RHS} \tag{32}$$

The right hand side is simplified by introduction of a function f defined by its transform $\widehat{RHS} = \widehat{F}\widehat{G}/(\Delta x)$. Making use of the aliasing theorem, relating the discrete transform with the continuous transform

$$\widehat{\mathcal{F}} = \sum_{m=-\infty}^{+\infty} \widetilde{\mathcal{F}}\left(k + \frac{2\pi m}{\Delta x}\right)$$

and the fact that the dispersion function $\widehat{W}$ is periodic, it can be shown that the following integral representation for ψ can be obtained,

$$\psi(x_m, t_n) = \frac{1}{4\pi^2}\int_{-\infty}^{+\infty} \mathrm{d}k \int_{-\infty}^{+\infty} \mathrm{d}\omega \; \frac{\widetilde{F}(k,\omega)}{\widehat{W}(k,\omega)}\, \mathrm{e}^{i(\omega n \Delta t - k m \Delta x)}. \tag{33}$$

The dispersion relation $\widehat{W} = 0$ becomes

$$\widehat{W} = \frac{\Delta x}{2\widehat{G}} - \frac{1}{g}\left(\frac{1}{(\Delta t)^2}\widehat{\mathcal{D}}^{(tt)} + \frac{U}{2\Delta x \Delta t}\widehat{\mathcal{D}}^{(t)}\widehat{\mathcal{D}}^{(x)} + \frac{U^2}{(\Delta x)^2}\widehat{\mathcal{D}}^{(xx)}\right) = 0 \tag{34}$$

with for the second order difference schemes

$$\begin{aligned}
\widehat{\mathcal{D}}^{(t)} &= 3 - 4\,\mathrm{e}^{-i\omega\Delta t} + \mathrm{e}^{-2i\omega\Delta t} \\
\widehat{\mathcal{D}}^{(tt)} &= 2 - 5\,\mathrm{e}^{-i\omega\Delta t} + 4\,\mathrm{e}^{-2i\omega\Delta t} - \mathrm{e}^{-3i\omega\Delta t} \\
\widehat{\mathcal{D}}^{(x)} &= d_{-1}^{(x)}\,\mathrm{e}^{-ik\Delta x} + d_0^{(x)} + d_1^{(x)}\,\mathrm{e}^{ik\Delta x} + d_2^{(x)}\,\mathrm{e}^{2ik\Delta x} \\
\widehat{\mathcal{D}}^{(xx)} &= d_{-1}^{(xx)}\,\mathrm{e}^{-ik\Delta x} + d_0^{(xx)} + d_1^{(xx)}\,\mathrm{e}^{ik\Delta x} + d_2^{(xx)}\,\mathrm{e}^{2ik\Delta x} + d_3^{(xx)}\,\mathrm{e}^{3ik\Delta x}
\end{aligned} \tag{35}$$

where the values of $d^{(xx)}$ and $d^{(x)}$ depend on the type of difference scheme, upwind or central. In analogy with the definition of $\widehat{k}$ we define $\widehat{\omega} = \frac{\omega\Delta t}{2\pi}$, the number of steps per waveperiod.

The discrete dispersion relation can be written as

$$\widehat{W} = -|k|\frac{\pi\widehat{k}}{(1-\varepsilon(\widehat{k}))\sin(\widehat{k}\pi)} - \frac{1}{g}\left(\frac{\omega^2}{4\pi^2\widehat{\omega}^2}\widehat{\mathcal{D}}^{(tt)} + \frac{2U\omega k}{16\pi^2\widehat{\omega}\widehat{k}}\widehat{\mathcal{D}}^{(t)}\widehat{\mathcal{D}}^{(x)} + \frac{U^2k^2}{4\pi^2\widehat{k}^2}\widehat{\mathcal{D}}^{(xx)}\right) = 0 \tag{36}$$

This dispersion relation is the most general one. We have discretized both the space and the time variable. It is also possible to derive relations for continuous time and discrete space variable etc.

For the computer program RAPID of Raven (1996) a comparison of the continuous and the discrete dispersion relation can be carried out by writing them in the form

$$\widetilde{\mathcal{W}}(k) = k_0\left(1 - 2\pi F n_{\Delta x}^2 \widehat{k}\right) \text{ and } \widehat{W} = k_0\left(1 - 2\pi F n_{\Delta x}^2 L h(\widehat{k})\right) \tag{37}$$

where k_0 is the fundamental wave number, $Fn^2_{\Delta x}$ the panel Froude number and $Lh(\widehat{k})$ a function including the Fourier transform of the Green's function, the difference scheme for the derivatives at the free surface, collocation points and the distance of the raised panels to the free surface. The analysis is carried out by plotting $Lh(\widehat{k})$ as a function of $\widehat{k}$. The intersection of the real part of $Lh(\widehat{k})$ with the line $1/Fn^2_{\Delta x}$ indicates the wavenumber of the discretized sheme and the imaginary part of $Lh(\widehat{k})$ is proportional to the numerical damping. This can be done due to the special form of their dispersion relation.

We shall write the zeros of the discrete dispersion relation in the following form

$$k_d = k_c\{1 + C_R(\omega, \Delta t, \Delta x) + iC_I(\omega, \Delta t, \Delta x)\}. \tag{38}$$

When the continuous wavenumber k_c is negative the wave is travelling upstream and when k_c is positive the wave is travelling downstream. The discrete wave numbers are the roots of the dispersion relation (36). The term C_R indicates numerical dispersion, an increase ($C_R < 0$) or decrease ($C_R > 0$) of the characteristic length of the associated waves. The term C_I indicates numerical damping ($C_I < 0$) or numerical amplification ($C_I > 0$). Usually one root is close to the continuous wavenumber. Any secondary root away from the continuous wave number indicates a spurious wave number. If the imaginary part of this root is positive, which means that the short waves with that wavelength will amplify rapidly, numerical instabilities, wiggles will appear.

Zero-speed

To get insight in the method we first study the zero-speed case. In this case the continuous dispersion relation (30) becomes

$$\widetilde{\mathcal{W}}(k,\omega) = -|k| + \frac{\omega^2}{g} = 0 \quad \Rightarrow \quad k_c = \frac{\omega^2}{g} \quad k > 0 \tag{39}$$

We shall compare this result with discrete models where we either have continuous time and discrete space or discrete time and continuous space or time and place discrete.

The discrete Fourier transform of the, continuous time and discrete space, dispersion relation reads

$$\widehat{W} = -|k| \frac{\pi\widehat{k}}{(1-\varepsilon(\widehat{k}))\sin(\widehat{k}\pi)} + \frac{\omega^2}{g} = 0 \qquad k > 0$$

In this case the analysis can be carried out in the same, however, we compute the zeros because in the most general case this is the only way to do it. In figure 7(a) we see that if we take more than 15 elements per wavelength, thus $\widehat{k} < 0.007$, the error due to numerical dispersion is less then 1%. The numerical damping or amplification is zero for all $\widehat{k}$. For the continuous space and discrete time case we have the dispersion relation

$$\widehat{W} = -|k| - \frac{\omega^2}{g} \frac{1}{4\pi^2\widehat{\omega}^2} \left(2 - 5\,\mathrm{e}^{-2\pi i\widehat{\omega}} + 4\,\mathrm{e}^{-4\pi i\widehat{\omega}} - \mathrm{e}^{-6\pi i\widehat{\omega}}\right) = 0 \qquad k > 0$$

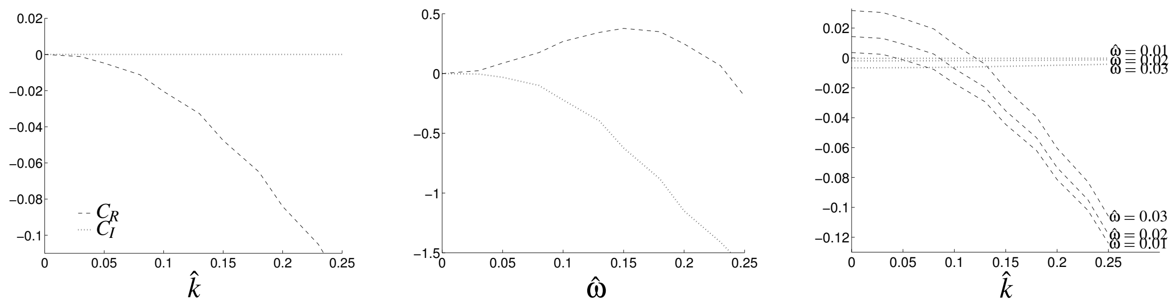

(a) Space discrete (b) Time discrete (c) Time and space discrete

Figure 7: The numerical dispersion C_R and damping C_I.

In figure 7(b), we see that $\widehat{\omega} < 0.025$ seems a good choice. In the case of both space and time discrete the dispersion relation becomes

$$\widehat{W}(k,\omega) = -|k|\frac{\pi\widehat{k}}{(1-\varepsilon(\widehat{k}))\sin(\widehat{k}\pi)} - \frac{\omega^2}{g}\frac{1}{4\pi^2\widehat{\omega}^2}\widehat{\mathcal{D}}^{(tt)} = 0 \qquad k > 0$$

with

$$\widehat{\mathcal{D}}^{(tt)} = 2 - 5\,\mathrm{e}^{-2\pi i\widehat{\omega}} + 4\,\mathrm{e}^{-4\pi i\widehat{\omega}} - \mathrm{e}^{-6\pi i\widehat{\omega}}$$

In figure 7(c) we see that for $\widehat{\omega} \leq 0.02$ and $0.04 \leq \widehat{k} \leq 0.12$ both the numerical dispersion and damping are small.

Waves and current

In this section, we compare the continuous dispersion relation (30) with speed for waves travelling downstream first, thus with the wave number:

$$k_c = \frac{g + 2U\omega \pm g\sqrt{1 + \frac{4U\omega}{g}}}{2U^2} \qquad k > 0\,, \tag{40}$$

with the discrete one (36). We look at the waves with the continuous wave number computed with minus the root ($-\sqrt{\;}$). Waves with the $+\sqrt{\;}$ have for small speed a very large wave number ($\approx g/U^2$), and therefore a very small wavelength. This wavelength is much smaller than the panel size.

We use either central discretization for the first- and second-order x-derivative, in equation (35),

$$d_n^{(x)} = \begin{cases} 1 & n = 1 \\ -1 & n = -1 \\ 0 & \text{elsewhere} \end{cases} \quad \text{and} \quad d_n^{(xx)} = \begin{cases} 1 & n = 1 \\ -2 & n = 0 \\ 1 & n = -1 \\ 0 & \text{elsewhere} \end{cases}\,, \tag{41}$$

or upwind discretization

$$d_n^{(x)} = \begin{cases} 3 & n=0 \\ -4 & n=-1 \\ 1 & n=-2 \\ 0 & \text{elsewhere} \end{cases} \quad \text{and} \quad d_n^{(xx)} = \begin{cases} 2 & n=0 \\ -5 & n=-1 \\ 4 & n=-2 \\ -1 & n=-3 \\ 0 & \text{elsewhere} \end{cases}. \tag{42}$$

In figures 8(a) and 8(b), we show the numerical dispersion C_R and damping C_I of these wave numbers as function of $\widehat{k}$. We see that for both discretizations for $\widehat{k} < 0.08$ both the numerical dispersion and damping are small, but there is more numerical damping using the upwind scheme. The upwind discretization for ψ_{xx}, figure 8(c) alone, gives poor results. Upwind discretization for ψ_x alone gives nearly the same result as in the case that we take for both ψ_{xx} and ψ_x upwind. We already mentioned the numerical instabilities which appear when we use central discretization and increase the speed. These instabilities appear when the discrete dispersion has an other root, larger than the original, therefore with a smaller wavelength. These secondary roots will cause numerical instabilities when the imaginary part is larger than zero, see equation (38). Using upwind discretization, the dispersion relation has one root, close to the continuous wave number. All possible spurious wave numbers have a very large negative imaginary part, therefore waves with that particular wavelength decay rapidly, or will not exist at all.

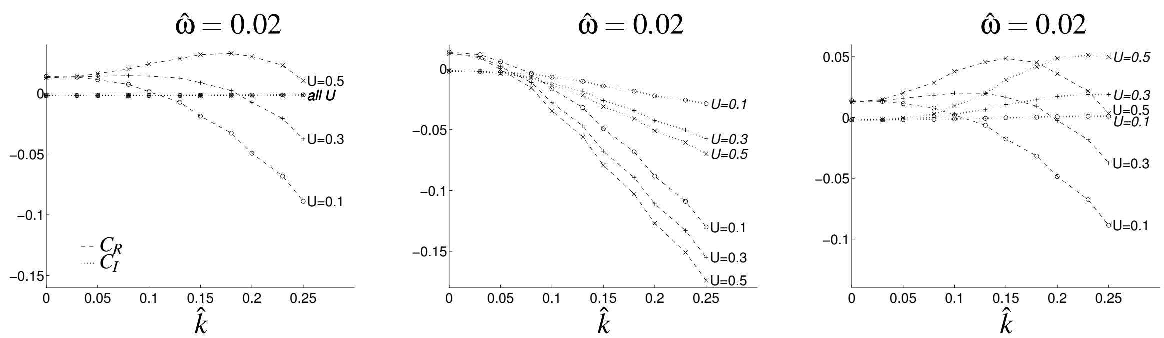

(a) Central (b) Upwind (c) ψ_{xx} upwind only

Figure 8: The numerical dispersion C_R and damping C_I for different difference schemes.

Using central discretization, the dispersion relation sometimes has two roots for one frequency, see figures 9(a) and 9(b). The solid lines are the wave number of the continuous dispersion relation, the same after we insert the results of figure 8(a) and 8(b) in (38). The root far from the continuous wave number has a very large imaginary part, which means that the short waves with that wavelength will amplify rapidly, therefore wiggles appear. Figure 9(a) shows, for instance, that when $\widehat{k} = 0.05$ and $U = 0.6$, wiggles are present for $\omega \geq 6$, and are absent for $\omega < 6$. The wave number of the spurious roots indicates a wavelength of about two panels. Trefethen (1982) explained that the group velocity, $\frac{\partial \omega}{\partial k}$ of the waves is essential to the study the instabilities. Our

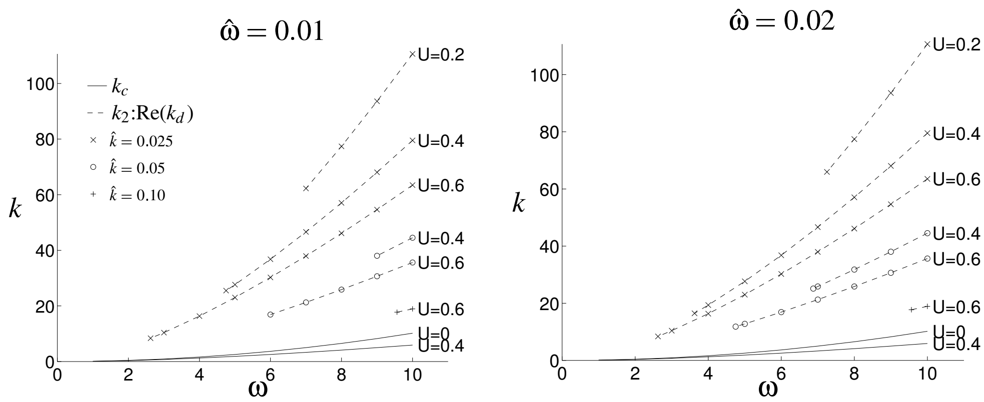

(a) (b)

Figure 9: The spurious wave number, as function of the frequency, for different $\widehat{k}$, different speeds U and for two values of ω, using central discretization.

problem is too complex to evaluate the group speed analytically, like Trefethen did. When looking at the slopes of the curves in figures 9(a) and 9(b), we see that the group velocity of the spurious waves is very small compared to that of the continuous waves. A small group velocity means that the energy does not radiate away, thus that the wave amplitude will increase. To prevent this type of instabilities Kim, Kring & Sclavounos (1997) apply a low-pass filter. Because the consequences of a low-pass filter on the actual wave are unknown and upwind discretization also prevent these instabilities, we will use upwind discretization. Figures 9(a) and 9(b) show that the existence of wiggles is dependent on the frequency ω, the speed U and the grid size Δx. The time step Δt seems to be not important. We now try to find a condition dependent on these quantities for which the wiggles are absent and thus the numerical scheme is stable. More precisely, we have to find a condition for which the discrete dispersion relation (36) has a complex root with a larger real part than the continuous root and with a positive imaginary part. It is not possible to derive this condition analytically, therefore we look at conditions which are mentioned in the literature. In figures 10(a) through 10(c), we try to derive a stability condition assuming that $\widehat{k}$ and $\widehat{\omega}$ are small enough to give an accurate representation of the first root, i.e. $\widehat{k} < 0.08$ and $\widehat{\omega} \leq 0.02$, see figure 8.

In figure 10(a), we show the maximum value of ω for which there are no wiggles. Therefore, for all frequencies under the lower line, for a particular U, $\widehat{k}$ and $\widehat{\omega}$, the central discretization is stable. We see that the condition is not only dependent on ω and U, but also of $\widehat{k}$ and therefore of Δx. It seems that the dependence on $\widehat{\omega}$ and Δt is not very important indeed. In figure 10(b), we show the maximum value of the critical grid Froude number $Fn_{\Delta x} = U/\sqrt{g\Delta x}$ for which there are no wiggles as function of U. This grid Froude number is used by Nakos (1990) and Raven (1996) in their analysis. In our analysis, the condition for stability seems to converge to $Fn_{\Delta x} = 0.3$, however it seems that there is still a dependence on the grid size or $\widehat{k}$. More compu-

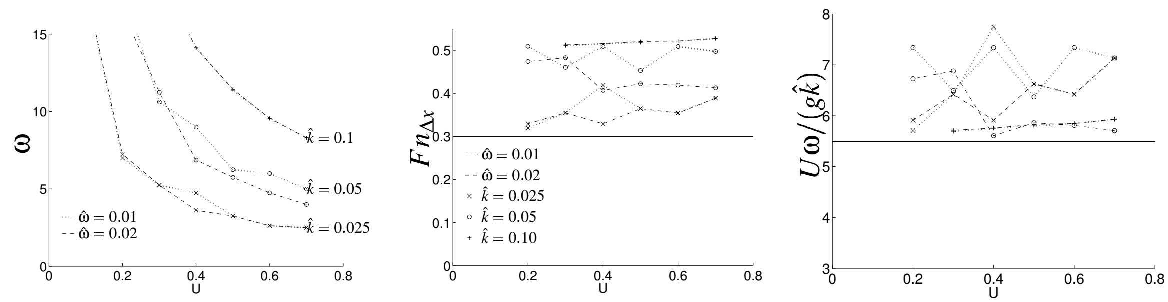

(a) Maximal ω (b) Maximal $Fn_{\Delta x}$ (c) Maximal $\frac{U\omega}{g\widehat{k}}$

Figure 10: The maximal values of several parameters for stable solutions

tations for smaller $\widehat{k}$ show the condition remains $Fn_{\Delta x} < 0.3$. In figure 10(c) we show the number $U\omega/(g\widehat{k})$. From this figure, we can say that if $U\omega/(g\widehat{k}) < 5.5$ the numerical scheme is stable. However, for smaller $\widehat{k}$ this condition becomes inaccurate, which can be seen from the oscillating behaviour of the plots for different $\widehat{k}$. On the whole, we may conclude that the best condition is: When the wave number is sufficiently accurate , thus $\widehat{k} < 0.08$ and $\widehat{\omega} \leq 0.02$, there is a chance that wiggles appear when $Fn_{\Delta x} > 0.3$. Using central discretization for the second derivative and upwind discretization for the first derivative, causes no numerical instabilities. The reverse, i.e. upwind ψ_{xx} and central ψ_x causes the same instabilities as both central.

If the waves travel in the opposite direction relative to the current we obtain similar results. The wave number becomes

$$k_c = \frac{-g + 2U\omega \pm g\sqrt{1 - \frac{4U\omega}{g}}}{2U^2} \qquad k < 0\,, \tag{43}$$

with the discrete one (36), for $k < 0$. We use the same discretizations as in the previous section. We only look at the wave numbers for which waves exist in the continuous case, thus for $\tau = U\omega/g < 0.25$. Figure 11 shows that the existence of wiggles upstream is also dependent on the frequency ω, the speed U, the grid size Δx. Figure 12 shows that the upstream side of the problem satisfies the condition $Fn_{\Delta x} < .25$. We mention that the spurious waves are travelling downstream, probably because the numerical errors amplify with the current downstream.

Steady forward speed

An extensive study op the properties of the Dawson and RAPID scheme has been carried out by Raven (1996). The dispersion relations for the 2D continuous and space-discrete case is written down in (37). The operator $Lh(\widehat{k})$ contains the effect of the choice of the relative forward shift (γ) of collocation point, the relative distance of the raised panels above the water surface (α) and the choice of the difference scheme. First the case that no errors are introduced by the difference

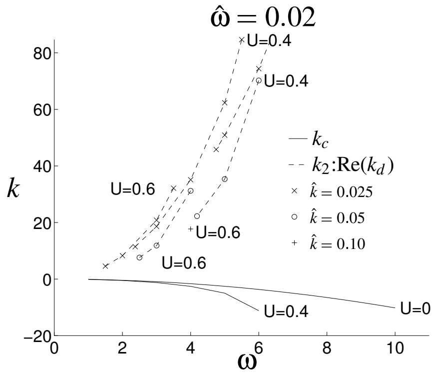

Figure 11: The spurious wave number, as function of the frequency, for different $\widehat{k}$, for $\widehat{\omega} = 0.01$ and for different speeds U, using central discretization.

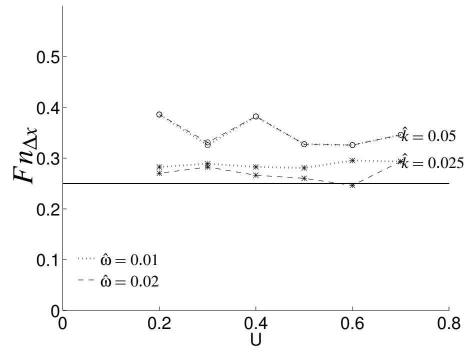

Figure 12: The maximum value of the grid Froude number, as function of U, $\widehat{k}$ and $\widehat{\omega}$, for which the central discretization is stable.

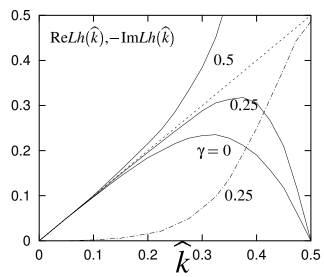

(a) $\alpha = 0.5$, no difference scheme

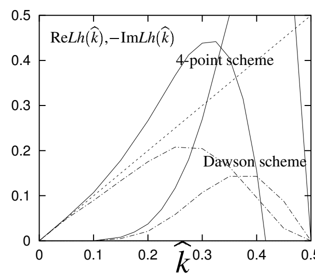

(b) $\alpha = 1.0, \gamma = 0.25$

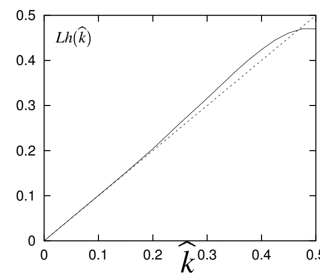

(c) Spline S2 scheme

Figure 13: $Lh(\widehat{k})$ for several choices of parameters and schemes

scheme is studied. In figure 13(a) for a fixed value of $\alpha = 0.5$ and for different values of γ the value of the real and imaginary part of $Lh(\widehat{k})$ are plotted against $\widehat{k}$. The continuous case results in the line $Lh(\widehat{k}) = \widehat{k}$. By visual inspection one sees that $\gamma = 0.25$ is a good choice. If one draws the line $Lh(\widehat{k}) = 1/(2\pi Fn^2_{\Delta x})$ one sees that the numerical dispersion is neglegible and the at the spurious wavelength the damping is large. The conclusion for other values of α is the same.

In figure 13(b) the effect of raised panel compared with a conventional distribution is shown. One sees that the raised panel method is superior even for the rather large value of $\alpha = 1.0$. One must realize that if one takes α to large the condition number of the matrix, to be inverted, becomes worse. If one takes $\widehat{k} < 0.1$ one sees that numerical dispersion is neglegible, while the damping at the spurious mode becomes very large.

Sclavounos et al (1988) presented the results obtained by means of a spline scheme instead of a difference scheme. Figure 13(c) shows that for their S2 scheme a good approximation of the continuous case over the entire range is obtained. One must keep in mind that in practical applications the value of $\widehat{k}$ is chosen rather small to obtain sufficient accuracy.

5 Results and discussion

Some of the practical results obtained by the methods explained will be shown. The frequency and time-domain methods explained in section three are used in the low speed region to compute the added mass and damping coefficients for some ship hulls. We present some of the

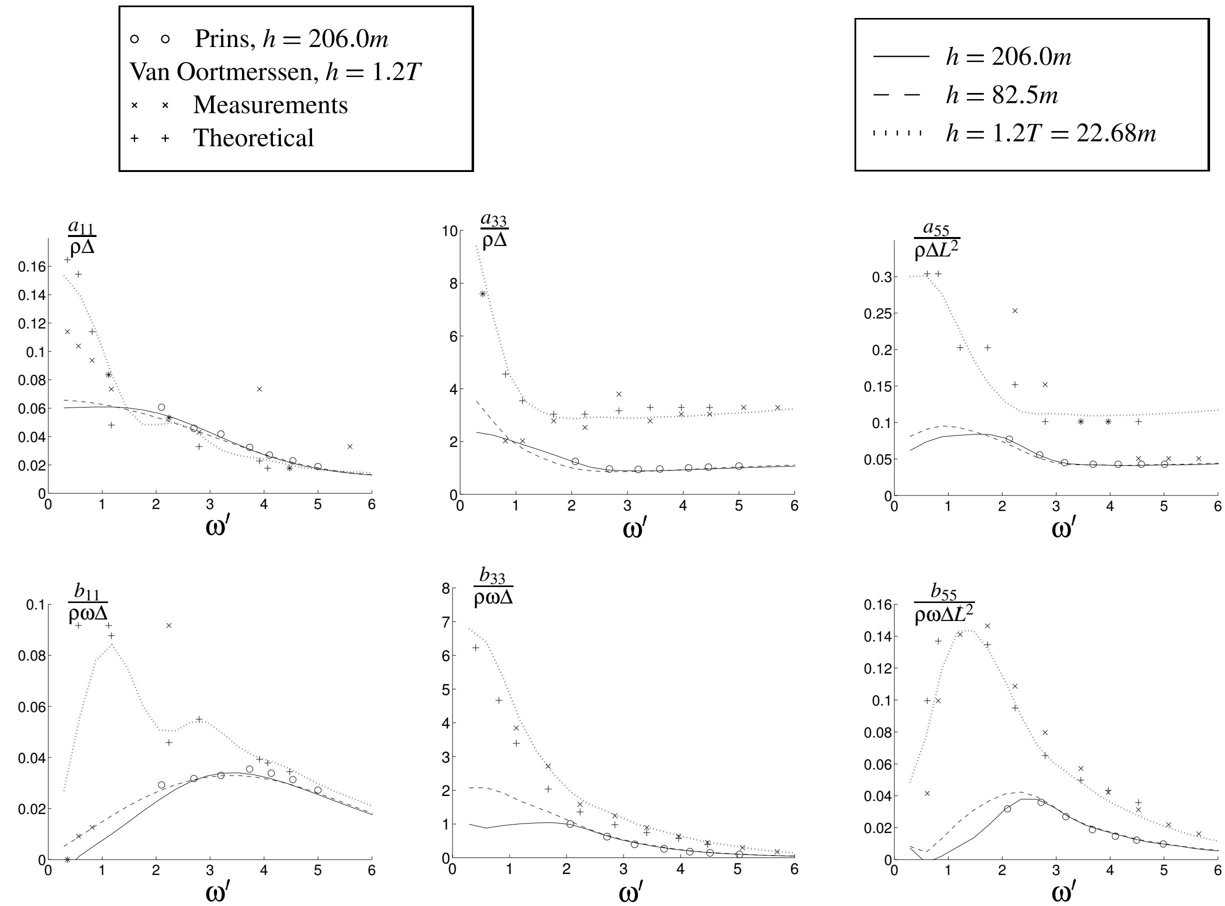

Figure 14: Added mass and damping coefficients for different water depth.

computational results for a 200kDWT tanker for which many experimental results are available at MARIN. Results are shown for the surge pitch, heave and pitch component. There are also results available for the rotational and coupling components. They are reported in the work of Huijsmans (1996), Prins (1995) and Sierevogel (1998). In figure (14) we compare added mass and damping coefficients at zero speed for several values of water depth. The drawn lines are results obtained by Sierevogel. Measurements of Van Oortmerssen (1976) for a rather small keel clearance are shown as well. The computations shown are carried out in the time-domain. With a special choice of the time signal for the forced motion the step response functions are obtained first. The shown coefficients are obtained by applying a Fourier transform to these functions. In this way a few computations are carried out to obtain the coefficients over a large frequency range.

To compute the second order constant wave-drift force in head seas one has to compute the

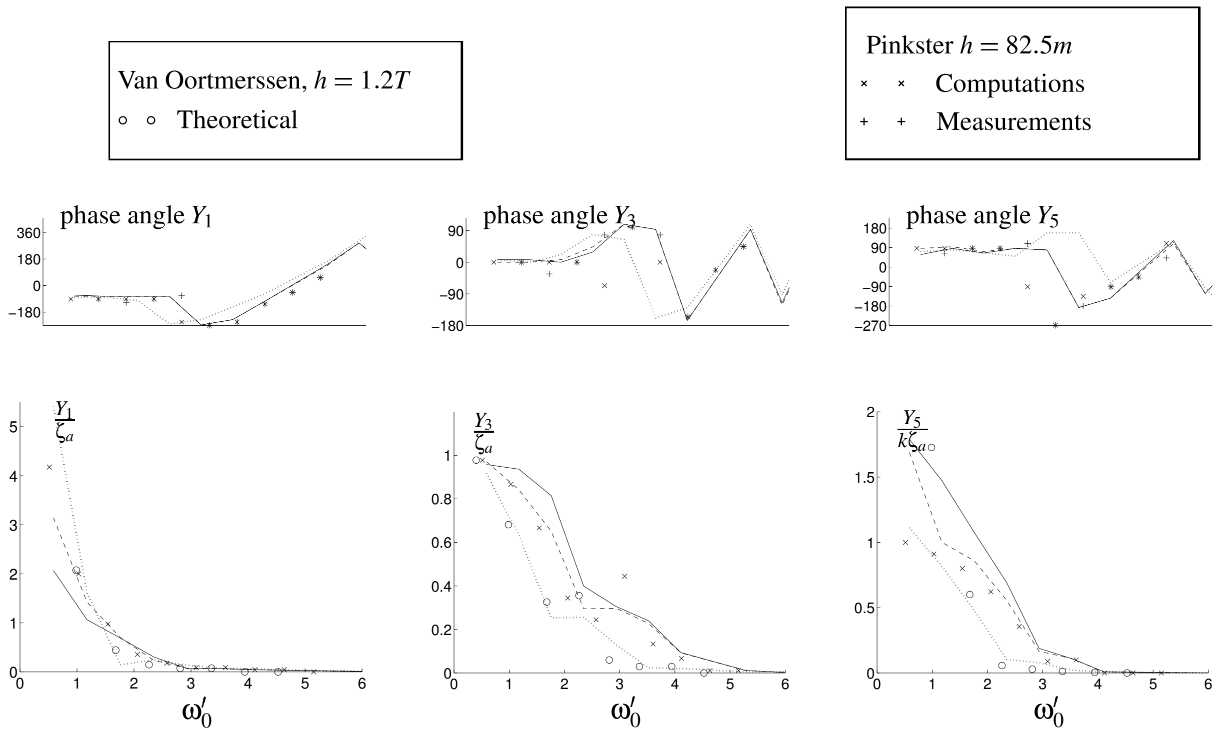

Figure 15: First-order motions in head waves, (legend for line styles see figure 14).

motion first. The second order drift force is well defined in the frequency domain. Hence, for each frequency the computation of the motion has to be repeated. For this reason the efficiency of the time-domain approach is less efficient. However to compute the second order low frequency motion one also has to compute the so called wave-drift damping coefficient. To compute this quantity one has to differentiate the wave-drift force with respect to the forward velocity at $U = 0$. To carry out this differentiaton numerically one has to compute the constant wave-drift force at low speed. This computation can be done by the program easely. A central difference scheme for the differentiation at the free surface is appropriate as shown in section 4. For this particular ship it is not advisable to use the Aranha (1994) approach.

$$b_{xx} = -\frac{\partial \overline{F}_x}{\partial U}|_{U=0} \approx k_0 \frac{\partial \overline{F}_x(\omega_0)}{\partial \omega_0} + \frac{4\omega_0}{g}\overline{F}_x(\omega_0) \tag{44}$$

To determine this approximation the values of the wave drift force at zero speed and its derivative with respect to frequency are sufficient. In the derivation of this formulation Aranha made several assumptions concerning the uniform behaviour of series expansions with respect to U. For certain applications not all these assumptions seem to be valid. Especially the speed dependent first order ship motions may destroy this uniformity. Near the peak of the wave-drift force curve the linearization of the wave motion with respect to U can not be carried out due to near resonance behaviour of the first order motions. For this reason numerical differentiation of the wave-drift force is the only way out. First we show the first order motions in figure (15).

First we compute the wave drift force. In figure (16) the results for the tanker are shown for several values of the water depth. The results shown in (17) are computations for three different objects, namely a hemisphere, VLCC and a LNG-carrier. There are not much experimental

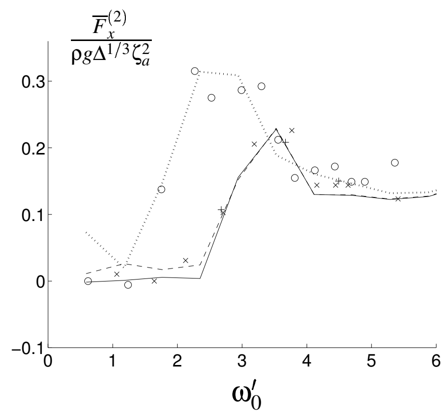

Figure 16: Drift forces in head waves (legend for line styles see figure 14), $+$ Wichers $h = 206m$, $\times$ Pinkster $h = 82.5m$ and $\circ$ Pinkster $h = 1.2T$.

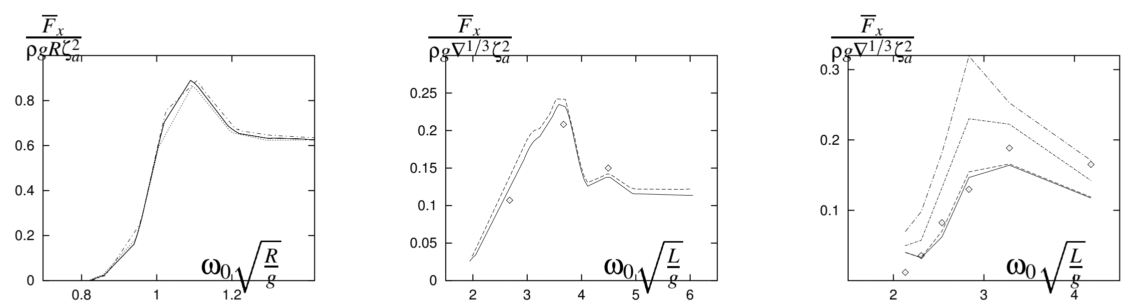

(a) Sphere, ——— $Fn = 0$, $\cdot - \cdot -$ $Fn = .005$, $\cdots$ $Fn = -.005$.

(b) Tanker, —— $Fn = 0$, $- -$ $Fn = 0.004$.

(c) LNG-carrier, —— $Fn = 0$, $- -$ $Fn = 0.003$, $--$ $Fn = 0.025$, $\cdot - \cdot -$ $Fn = 0.05$.

Figure 17: Wave-drift forces with measurements of Wichers (1988) $\diamond$.

results available for second order drift (or added resistance force) at low forward speed. The measurements of Wichers (1988) presented here are carried out at zero forward speed.

For the computation of the second order low frequency motion the value of the damping must be available. This damping term consists of a viscous and a potential part. If the wave height is large then the influence of the potential part becomes dominant, due to the fact that it is proportional to the square of the wave height. So in survival conditions it is important to know its value. In figure 18 the results are presented of computations of this damping coefficient. In the first two figures also results are shown obtained by means of the formula (44) derived by Aranha (1994). In the figure for the hemisphere the last part in (44) is presented as well. For the tanker

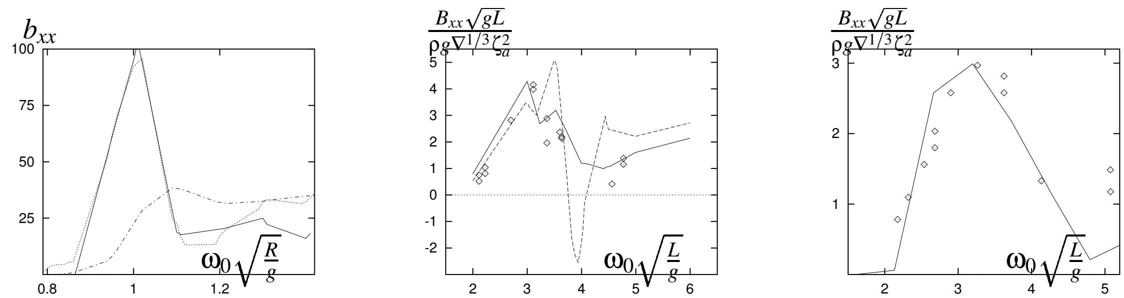

(a) Sphere, $\cdots$ approx., $\cdot - \cdot -$ partial, —— direct.

(b) Tanker, $---$ direct, $--$ approx.

(c) LNG-carrier, —— direct.

Figure 18: Wave-drift damping with measurements of Wichers (1988) $\diamond$.

the approximate results of Aranha are good for $\omega_0\sqrt{L/g} < 3.2$. The contribution of first order motion terms to the wave drift force generates the large negative derivatives over the peak of the force, this gives rise to the non realistic negative values of the approximate formulation. In many severe operational conditions the values the results of Aranha can be used. The computed results agree well with the mesurements carried out of Wichers (1988) for both ships.

References

B. V. Korvin-Kroukovsky and W. R. Jacobs (1957), Pitching and heaving motions of a ship in regular waves, *Trans. SNAME* 65 590-632.

J. L. Hess and A. M. O. Smith, (1962), *Calculation of non-lifting potential flow about arbitrary three-dimensional bodies*, Douglas Aircraft Company, Report No. 40622.

H. C. Raven, (1996), *A Solution Method for the Nonlinear Ship Wave Resistance Problem*, Doctor Thesis, TU Delft, 220 pages.

R. H. M. Huijsmans, (1996), *Mathematical Modelling of the Mean Wave Drift Force in Current, a numerical and experimental study*, Doctor Thesis, TU Delft, 187 pages.

H. J. Prins, (1995), *Time-Domain Calculations of Drift Forces and Moments*, Doctor Thesis, TU Delft, 154 pages.

L. M. Sierevogel, (1998), *Time-Domain Calculations of Ship Motions*, Doctor Thesis, TU Delft, 134 pages.

T. H. J. Bunnik and A. J. Hermans, (1998), Stability analysis for solving the 3D unsteady free-surface condition with raised panels, *Proc. of the 13th IWWWFB*, ISBN 90-407-1673-0, 13-16.

K. Eggers, (1981), Non-Kelvin dispersive waves around non-slender ships, *Schiffstechnik* 28 223-251.

A. J. Hermans and P. H. van Gemert, (1989), A linear surface condition in low speed hydrodynamics, *Ship Technology Research (Schifftechnik)* 36 181-196.

F. J. Brandsma, (1987), *Low Froude Number Expansions for the Wave Pattern and the Wave Resistance of General Ship Forms*, Doctor Thesis, TU Delft, 111 pages.

E. Baba, (1976), *Wave resistance of ships in low speed*, Mitsubishi Technical Bulletin 109.

C. W. Dawson, (1977), A practical computer method for solving ship-wave problems, *Proc. 2nd Int. Conf. Numerical Ship Hydrodynamics*, 30-38.

J. N. Newman, (1985). Algorithms for the free-surface Green function, *J. of Engineering Mathematics*, 19 57-67.

J. N. Newman, (1992). The approximation of free-surface Green functions, *Wave Asymptotics*, eds. P.A. Martin and G.R. Wickham, Cambridge University Press, 107-135.

F. Noblesse, (1982), The Green function in the theory of radiation and diffraction of regular water waves by a body, *J. of Engineering Mathematics*, 16 137-169.

R. W-C. Yeung, (1973), *A Singularity-Distribution Method for Free-Surface Flow Problems with an Oscillating Body*, Technical Report NA 73-6, College of Engineering, University of California, Berkeley.

A. J. Hermans and R. H. M. Huijsmans, (1987), The effect of moderate speed on the motions of a floating body, *Schiffstechnik*, 34 132-148.

J. B. Keller and D. Givoli, (1989), Exact non-reflecting boundary conditions, *J. of Computational Physics*, vol. 82, 172-192.

D. Givoli, (1992), *Numerical methods for problems in infinite domains*, Elsevier, Amsterdam.

D. E. Nakos, (1990), *Ship Wave Patterns and Motions by a Three-Dimensional Rankine Panel Method*, PhD Thesis, MIT.

L. N. Trefethen, (1982), Group velocity in finite difference schemes, *Siam Review*, 24 113-136.

Y. Kim, D. C. Kring and P. D. Sclavounos, (1997), Linear and nonlinear interaction of surface waves with bodies by a three-dimensional Rnkine panel method, submitted for publ.

P. D. Sclavounos and D. E. Nakos, (1988), stability analysis of panel methods for free-surface flows with forward speed, *Proc. 17th Symp. on Naval Hydrodynamics*, 173-195.

G. van Oortmerssen, (1976), *The Motions of a Moored Ship in Waves*, Doctors Thesis, TU Delft, 141 pages.

J. A. P. Aranha, (1994). A formulation for 'wave damping' in the drift for a floating body, *J. of Fluid Mechanics*, 275, 147-155.